Generation of integer and fractional vector beams with q-plates encoded onto a spatial light modulator

IGNACIO MORENO,[1] MARÍA M. SANCHEZ-LOPEZ,[2,*] KATHERINE BADHAM,[3] JEFFREY A. DAVIS,[3] AND DON M. COTTRELL[3]

[1]*Departamento de Ciencia de Materiales, Óptica y Tecnología Electrónica. Universidad Miguel Hernández, 03202 Elche, Spain*
[2]*Instituto de Bioingeniería y Departamento de Física y Arquitectura de Computadores, Universidad Miguel Hernández, 03202 Elche, Spain*
[3]*Department of Physics, San Diego State University, San Diego, CA 92182-1233, USA*
**Corresponding author: mar.sanchez@umh.es*

Received XX Month XXXX; revised XX Month, XXXX; accepted XX Month XXXX; posted XX Month XXXX (Doc. ID XXXXX); published XX Month XXXX

http://dx.doi.org/10.1364/OL.41.001305

We generate programmable vector beams with arbitrary *q*-plates encoded using a spatial light modulator system. Consequently we can analyze new and exotic *q*-plate designs without the difficulty of fabricating individual plates. We show experimental results for positive and negative integer and new fractional vector beam values.

OCIS codes: *(230.3720) Liquid-crystal devices; (230.5440) Polarization-selective devices; (120.5410) Polarimetry.*

http://dx.doi.org/10.1364/OL.99.099999

Optical retarder elements with azimuthal rotation of the principal axes are receiving a great deal of attention due to their ability to create cylindrically polarized vector beams, and to transfer orbital angular momentum (OAM) to light [1]. In addition, both OAM and vector beam multiplexing are being investigated as promising new techniques for optical communications [2-5]. Among the devices studied have been *q*-plates [6,7], which are half-wave retarders where the principal axis rotates with the azimuth angle θ as $q\theta$. Typical values are q=1/2 and q=1, where the principal axis rotates through π radians and through 2π radians respectively [6,7]. These devices can be fabricated with special liquid crystal (LC) patterns [8], where the retardance can be tuned electronically. However the orientation of the LC director axes remains fixed, with the q-value defined in the fabrication design.

These devices produce higher order cylindrically polarized vector fields with a polarization state that varies spatially with axial symmetry [9]. Such cylindrically polarized vector beams can be represented in the higher order Poincaré spheres [10-12]. We have demonstrated a potentially high-speed system for switching states within the generalized Poincaré sphere [13,14].

In this work we show a polarization system using a single spatial light modulator (SLM) that allows the configuration of arbitrary *q*-plates. We show results that demonstrate the ability of the proposed system to reproduce previous *q*-plate devices; but also new *q*-plate designs producing fractional vector beams.

First, we apply a representation of the *q*-plate Jones matrix that shows the mathematics behind our system. We use a quarter-wave plate (QWP) oriented at 45º, followed by a device with one spiral phase of charge ℓ affecting one linear polarization and another opposite spiral phase affecting the orthogonal polarization, followed by another QWP oriented at -45º and a half-wave plate (HWP) vertically oriented. This can be written in a Jones matrix form as

$$\mathbf{M}_{\ell}(\theta)=\mathbf{W}(\pi)\mathbf{W}(\pi/2,-45^{\circ})\mathbf{W}(\ell\theta)\mathbf{W}(\pi/2,+45^{\circ}). \quad (1)$$

Here, the rotated QWP is given by the product $\mathbf{W}(\pi/2,\pm45^{\circ})=\mathbf{R}(\mp45^{\circ})\mathbf{W}(\pi/2)\mathbf{R}(\pm45^{\circ})$, where the rotation and aligned linear retarder matrices are given as:

$$\mathbf{R}(\theta)=\begin{pmatrix}\cos(\theta) & \sin(\theta)\\ -\sin(\theta) & \cos(\theta)\end{pmatrix}, \qquad \mathbf{W}(\phi)=\begin{pmatrix}e^{i\phi/2} & 0\\ 0 & e^{-i\phi/2}\end{pmatrix}. \quad (2)$$

The matrix $\mathbf{W}(\ell\theta)$ represents a special aligned linear retarder with two opposite spiral patterns that affect the vertical and horizontal polarizations, so the retardance changes azimuthally as $\phi=2\ell\theta$ and

$$\mathbf{W}(\ell\theta)=\begin{pmatrix}e^{i\ell\theta} & 0\\ 0 & e^{-i\ell\theta}\end{pmatrix}. \quad (3)$$

Thus, the product in Eq. (1) gives the general matrix for a *q*-plate [6] as:

$$\mathbf{M}_{\ell}(\theta)=\begin{pmatrix}\cos(\ell\theta) & \sin(\ell\theta)\\ \sin(\ell\theta) & -\cos(\ell\theta)\end{pmatrix}. \quad (4)$$

Therefore, it can be used to generate vector beams in the Poincaré sphere of order $\ell=2q$. However, this approach requires the capability to independently spatially modulate the two linear components of the electric field for the matrix in Eq. (3). This cannot be achieved with a single LC-SLM because only one linear polarization component (parallel to the LC director) will be modulated.

Here we use a previously reported experimental setup [15], designed to modulate the two orthogonal linear polarization components as shown in Fig. 1. We use a transmissive parallel-aligned LC-SLM. The LC director is oriented vertically, and therefore the vertical polarization component is phase modulated, while the horizontal component is unaffected.

The LC-SLM screen is divided in two halves, where two different spiral phase patterns are addressed, each with a radius of N=120 pixels as shown in Fig. 1. The initial beam illuminates only the left half of the screen where the spiral phase pattern, having a charge ℓ, is encoded onto the vertical polarization component. The horizontal component is perpendicular to the LCD director axis and is unaffected. Then, by means of a lens (L) and a mirror (R), the beam is reflected back to the right part of the LC-SLM. The initially vertical and horizontal polarization components are reversed by the insertion of the quarter-wave plate QWP2, oriented at 45º with respect to the LC director axis. Now the horizontal polarization component, which was not affected by the LCD in the initial passage, becomes vertically polarized and will be modulated by the second spiral phase pattern encoded on the right side of the LC-SLM.

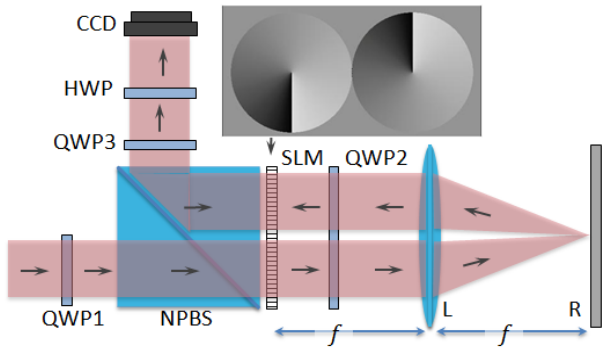

Fig. 1. Double pass system to generate generic q-plates.

Note that the focusing lens and mirror in Fig. 1 comprise a 4f imaging system and that the initial vertical polarization is converted into the horizontal polarization. As a result, the left side of the SLM encodes the positive spiral phase $\exp(+i\ell\theta)$ while the right side encodes the negative spiral phase $\exp(-i\ell\theta)$ and the matrix of Eq. (3) is formed. The inset in Fig. 1 shows the type of pattern encoded onto the LC-SLM. The phase masks are flipped to compensate for the 4f imaging system discussed earlier. The output beam is selected using a non-polarizing beam splitter (NPBS). Because we are using a 4f system to image the first spiral phase pattern onto the second, there are no manifestations of the Gouy phase effects [16].

Finally, in order to complete the system in Eq. (1), we added QWP1 at the input, and QWP3 and HWP at the output from the NPBS. Note that a related system was employed earlier to generate radial and azimuthal polarization [17]. However, including the initial QWP and the final HWP allow the exact reproduction of the q-plate in Eq. (4). Therefore, it can be used to program generic q-plates and use them to generate vector beams of any Poincaré sphere of arbitrary order.

To verify the generation of these vector beams, we need to control the input polarization. We use a polarization state generator (PSG) system reported earlier [13,14], which could be electronically controlled at GHz speeds using electro-optic retarders.

The versatility of the q-plate equivalent system is shown in Fig 2. In this figure output vector beams with different integer orders are displayed. In order to verify the polarization pattern of the output beam, different analyzers are placed before the CCD: a linear polarizer oriented at 0º, 45º, 90 and 135º, and right (RCP) and left (LCP) circular polarizers. In all cases the input beam was selected with a fixed vertical linear polarization. Fig. 2(a) shows results where we generate a charge of $2q$=+1. In this case, the spiral phases are adjusted to generate the radial polarized beam. These results agree with previous reports [17]. In particular, we see that the direction of the linearly polarized output follows the orientation of the analyzer. Fig. 2(b) shows the case when the charge is changed to $2q$=-1. The main difference as we reverse the charge occurs when the analyzer polarizer is rotated. In Fig. 2(a), we saw that the bright area rotated in the same direction as the analyzer. By contrast, for the negative charge, the bright area rotates in the opposite direction as the analyzer. This can be explained using the expected polarization pattern on the left column.

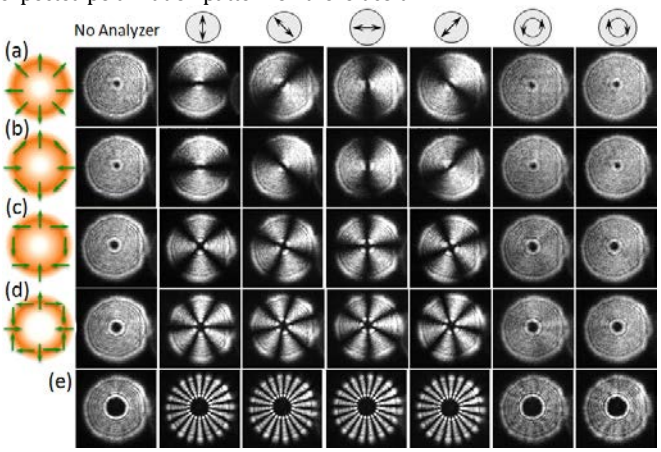

Fig. 2. Generation of integer order vector beams with different encoded q-plates: (a) $2q$=+1, (b) $2q$=-1, (c) $2q$=+2, (d) $2q$=+3, (e) $2q$=+10. Input polarization is vertical linearly polarized in all cases.

Figures 2(c), 2(d), and 2(e) show cases where the vector beam has orders of $2q$=2, $2q$=3 and $2q$=10. There are two main differences. First, when the linear analyzer is selected, we see 4, 6 and 20 bright lobes respectively. In addition when detecting the circular components, we see the size of the center singularity becomes larger as the topological charge increases. Note that these kinds of intensity patterns have been reported earlier [17]. But the novelty here is that we generate them by encoding arbitrary q-plates in the SLM system. Therefore, we have the capability to switch the order of the vector beam by changing the pattern addressed to the SLM. And for a given fixed order, we can generate any vector beam in the corresponding generalized Poincaré sphere by changing the input polarization.

We note that other approaches such as in [18] have been reported for the generation of vector beams, mostly using LCOS reflective devices rather than our parallel-aligned transmissive device [19]. Major difference between the two approaches is the poor extinction ratio of many LCOS devices that result in a strong DC term [20]. Consequently these architectures require the encoding of gratings onto the patterns to separate the desired information. We do not require this as seen in Fig. 2. A strong DC component would show up at the center of the vector beam outputs where the strong dark spot is easily seen. Our device has a measured extinction radio of better than -25 dB.

It is interesting to re-interpret these standard vector beams in Fig. 2 with a different point of view that considers the polarization rotation as a retardance between the RCP and LCP polarization components. This is shown in Fig. 3, where we analyze the $2q$=+1 case. For this q value, the phase increases azimuthally counterclockwise from 0 to 2π for the

LCP component, while it increases clockwise from 0 to 2π for the RCP component. This is indicated as the blue and red curves in Fig. 3.

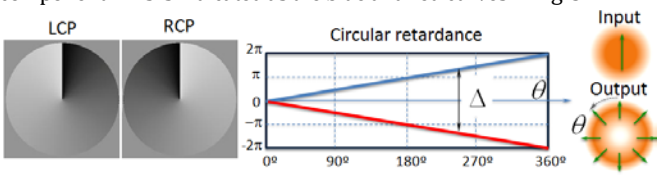

Fig. 3. Interpretation of the vector beam generator as an azimuthal retarder between RCP and LCP states.

Therefore, the retardance Δ between the circular components (circular retardance) increases with the azimuth as 2θ. Note that there is no phase discontinuity. The polarization rotation grows as $\Delta/2$ [21]. Therefore, the polarization at the origin (θ=0) is rotated azimuthally by 360º, as indicated on the right part of Fig. 3, thus creating the radial polarization output. For higher values of q, the circular retardance Δ grows faster with the azimuth, thus producing faster rotations that explain the other polarization maps in Fig. 1. However, there is no phase discontinuity for integer values of $2q$.

Our approach allows the generation of new cases with fractional vector charges with interesting results. The idea behind this approach can be understood by examining the circular retardance Δ for the case $2q$=1/2, which now increases linearly with the azimuth angle as shown in Fig. 4. Note that now there is a phase discontinuity at the origin. Consequently, the polarization rotation grows as $\Delta/2=\theta/2$, and the input polarization only rotates by 180º in the complete azimuthal range. As a result, there is a discontinuity in the state of polarization at the origin, which shows an opposite sense of the electric field depending whether we approach from θ=0 or from $\theta=2\pi$.

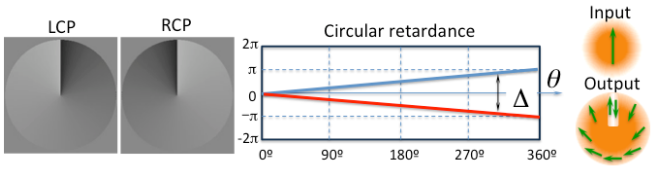

Fig. 4. LCP and RCP phase variation versus azimuthal angle for the case of $2q$=1/2 and example of the generation of a vector beam

Figure 5 shows experimental results for six different input polarizations: linear vertical, at +45º, horizontal, and at 135º, and RCP and LCP. They lead to six different output polarization patterns drawn on the left column of Fig. 5. These outputs have several features. First, a dark line appears through half of the output, due to the phase discontinuity that occurs at the azimuthal angle θ=0. Since now the phase changes azimuthally only from 0 to π, there is a π phase discontinuity at this angle. Note that this phase discontinuity happens for both the RCP and LCP components in all cases, as shown when the beams are analyzed with the circular analyzers (see the last two columns). Finally, the last two rows verify the operation of the q-plate by the conversion of RCP to LCP and the reverse.

Note that, when the input polarization is linear (cases 5(a) to 5(d)), the same output polarization, but with opposite sense, is obtained on each side of the dark vertical line, depending whether we approach to θ=0 from the left, or to $\theta=2\pi$ from the right. Therefore, the polarization at the origin is the same, but the phase discontinuity results in opposite sense of electric field on each side.

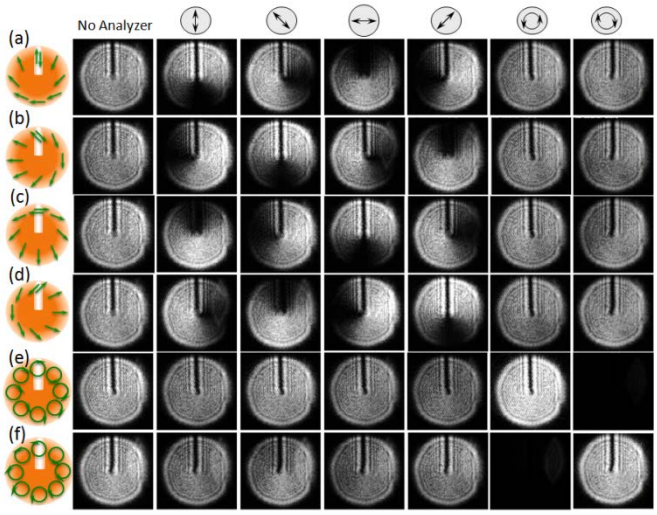

Fig. 5. Fractional $2q$=1/2 vector beams showing the output intensity for various input polarization states and output analyzers.

This explanation of the polarization maps reveals more interesting effects. For instance, Fig. 6 shows results where we produce an azimuthal phase variation of 3π in both orthogonal polarization components. But instead of using a continuous phase from zero to 3π, that would be the case for the standard $2q$=3/2 plate, we make three angular sectors where the phase grows from zero to π. Now the LCP and RCP phase difference linearly grows from zero to 2π in each sector of 120º, thus producing a total azimuthal polarization rotation of 180º in each sector. Therefore, the polarization at the border lines of each sector is the same, but the phase discontinuity results in opposite sense of electric field on each side.

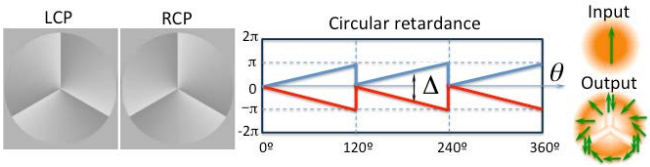

Fig. 6. LCP and RCP phase variation versus azimuthal angle for $2q$=3/2 with three angular sectors with phases changing 0 to π.

Again in Fig. 7 we show the corresponding experimental results for this exotic q-plate, for the same six input polarizations: linear vertical, at +45º, horizontal, at 135º, and RCP and LCP polarizations. They generate different polarization maps indicated on the left column, which are derived as before, by calculating the polarization rotation as half the circular retardance Δ.

Now we see three dark lines at azimuth angles 0º, 120º and 240º. They correspond to the phase discontinuities that occur at intervals of 120º for the two phase patterns encoded by the LC-SLM. The intensity distributions agree in all cases with the projection of the states of polarization drawn on the left column to the corresponding analyzer.

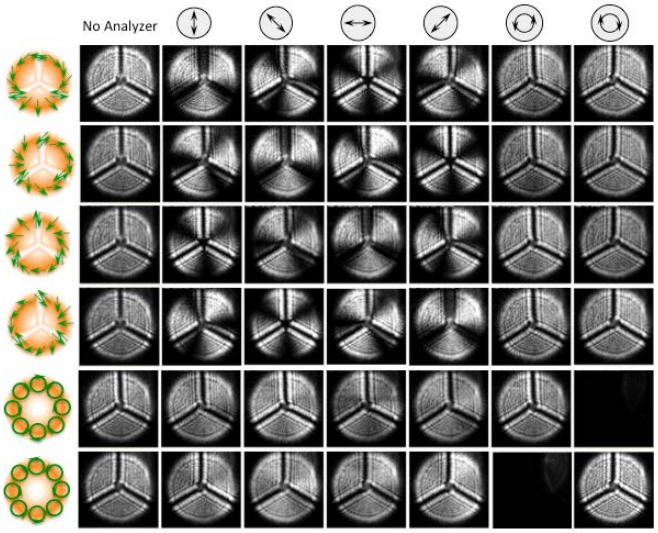

Fig. 7 Generation of vector beams for a fractional $2q$=3/2 made of three 0 to π phase sectors. Here the output intensity is shown for various input polarization states and various output analyzers.

Finally, since we have freedom in selecting the origin of each phase pattern, we can select the placement and number of the dark lines as shown in Fig. 8. Here we rotate the phase maps by a given angle to rotate the dark lines. For instance, in Fig. 8(a) and 8(b) we rotate both phase patterns shown in Fig. 5 ($2q$=1/2), but in opposite sense, by 45º and by 90º respectively. The corresponding polarization maps drawn in the left column are derived with the same technique as previously. Or we can rotate only one phase pattern to double the number of dark lines, as shown in Fig. 8(c). This corresponds to the case in Fig. 7, but is modified by rotating one phase pattern by 120º. Now six dark lines appear every 60º corresponding to the phase discontinuities. Again, the intensity distributions agree in all cases with the projection of polarization states onto the corresponding analyzer.

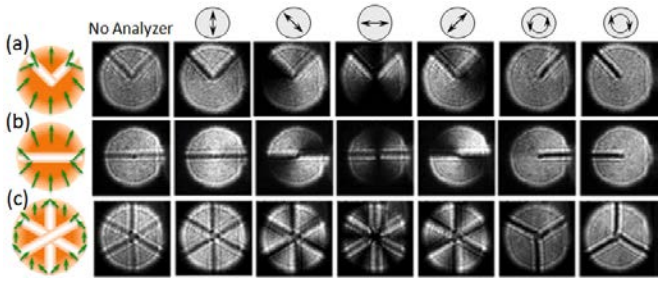

Fig. 8. Polarization map and intensity patterns for $2q$=1/2 with phase origins rotated by (a) 45º and (b) 90º, and (c) for $2q$=3/2 with rotation of one phase pattern by 120º.

In conclusion, we have developed a programmable system that allows the generation of arbitrary vector beams with generic q-plates encoded onto a SLM. We have proved it by reproducing standard q-plates that generate vector beams of orders $2q$=1 and $2q$=2, and verified their polarization conversion properties. We reproduced also the negative $2q$=-1 device, as well as other higher order values .

Then we also proposed and experimentally verified some new q-plate designs that produce vector beams with fractional orders. We tested the fractional value $2q$=1/2, and verified the formation of a line of phase discontinuity. Then we further explored this approach by designing a special case of a $2q$=3/2, but instead of having a continuous azimuthal phase it shows three sectors where the phase changes from 0 to π The result is a pattern with three line discontinuities. Obviously higher fractional values for $2q$ produce more phase discontinuities.

We provided an explanation of the vector beam generation in terms of the azimuthal variation in the retardance between the RCP and LCP components that gives intuitive insight into the polarization pattern generated by the q-plate design.

As stated earlier, this system allows rapid analysis of exotic vector beams prior to more expensive fabrication of the q-plate designs generating them. The fractional vector beams with dark lines shown here might be useful in advanced trapping applications. In addition, these fractional vector beams might encode additional information onto optical communication systems.

Funding. Ministerio de Ciencia e Innovación from Spain (FIS2012-39158-C02-02).

References

1. A. M. Yao, and M. J. Padget, Adv. Opt. Photon. **3**, 161–204 (2011).
2. J. Wang, J.-Y. Yang, I.M. Fazal, N. Ahmed, Y. Yan, H. Huang, Y. Ren, Y. Yue, S. Dolinar, M. Tur, and A.E. Willner, Nat. Photonics **138**, 488-496 (2012).
3. N. Bozinovic, Y. Yue, Y. Ren, M. Tur, P. Kristensen, H. Huang, A.E. Willner, and S. Ramachandran, Science **340**, 1545-1548 (2013).
4. G. Milione, M. P. J. Lavery, H. Huang, Y. Ren, G. Xie, T. A. Nguyen, E. Karimi, L. Marrucci, D. A. Nolan, R. R. Alfano, and A. E. Willner, Opt. Lett. **40**, 1980-1983 (2015).
5. G. Milione, T. A. Nguyen, J. Leach, D. A. Nolan, and R. R. Alfano, Opt. Lett. **40**, 4887-4890 (2015).
6. L. Marrucci, C. Manzo, and D. Paparo, Phys. Rev. Lett. **96**, 163905 (2006).
7. M. Beresna, M. Gecevičius, P. G. Kazansky, and T. Gertus, Appl. Phys. Lett. **98**, 201101 (2011).
8. S. Slussarenko, A. Murauski, T. Du, V. Chigrinov, L. Marrucci, and E. Santamato, Opt. Express **19**, 4085-4090 (2011).
9. Q. Zhan, Adv. Opt. Photon. **1**, 1–57 (2009).
10. G. Milione, H. I. Sztul, D. A. Nolan, and R. R. Alfano, Phys. Rev. Lett. **107**, 053601 (2011).
11. S. Chen, X. Zhou, Y. Liu, X. Ling, H. Luo, and S. Wen, Opt. Lett. **39**, 5274-5276 (2014).
12. E. Karimi, S. Slussarenko, B. Piccirillo, L. Marrucci, and E. Santamato, Phys. Rev. A **81**, 053813 (2010).
13. J. A. Davis, N. Hashimoto, M. Kurihara, E Hurtado, M. Pierce, M. M. Sánchez-López, K. Badham, and I. Moreno, Appl. Opt. **54**, 9583-9590 (2015).
14. M. M. Sánchez-López, J. A. Davis, N. Hashimoto, I. Moreno, E. Hurtado, K. Badham, A. Tanabe, and S. W. Delaney, Opt. Lett. **41**, 13-16 (2016).
15. I. Moreno, J.A. Davis, T.M. Hernandez, D.M. Cottrell, and D. Sand, Opt. Express **20**, 364-376 (2012).
16. G. M. Philip, V. Kumar, G. Milione, and N. K. Viswanathan, Opt. Lett. **37**, 2667-2669 (2012).
17. I. Moreno, J. A. Davis, D.M. Cottrell, and R. Donoso, Appl. Opt. **53**, 5493-5501 (2014).
18. C. Maurer, A. Jesacher, S. Furhapter, S. Bernet, and M. Ritsch-Marte, New J. Phys. **9**, 1-19 (2007).
19. J. A. Davis, P. Tsai, D. M. Cottrell, T. Sonehara, and J. Amako, Opt. Eng. **38**, 1051-1057 (1999).
20. A. Dudley, G. Milione, R. R. Alfano, and A. Forbes, Opt. Express **22**, 14031-14040 (2014).
21. J. A. Davis, D. E. McNamara, D. M. Cottrell, and T. Sonehara, Appl. Opt. **39**, 1549–1554 (2000).